



Heterogeneous & Homogeneous & Bio- & Nano-

CHEM **CAT** CHEM

CATALYSIS

Accepted Article

Title: Self-organization of ionic liquid-modified organosilica hollow nanospheres and heteropolyacids: efficient preparation of 5-HMF under mild conditions

Authors: Sai An, Zelin Wang, Huaiying Zhang, Haralampos N. Miras, and Yu-Fei Song

This manuscript has been accepted after peer review and appears as an Accepted Article online prior to editing, proofing, and formal publication of the final Version of Record (VoR). This work is currently citable by using the Digital Object Identifier (DOI) given below. The VoR will be published online in Early View as soon as possible and may be different to this Accepted Article as a result of editing. Readers should obtain the VoR from the journal website shown below when it is published to ensure accuracy of information. The authors are responsible for the content of this Accepted Article.

To be cited as: *ChemCatChem* 10.1002/cctc.201900285

Link to VoR: <http://dx.doi.org/10.1002/cctc.201900285>

WILEY-VCH

www.chemcatchem.org



Self-organization of ionic liquid-modified organosilica hollow nanospheres and heteropolyacids: efficient preparation of 5-HMF under mild conditions

Dr. Sai An^a, Zelin Wang^a, Huaiying Zhang^a, Dr. Haralampos N. Miras^{*b} and Prof. Dr. Yu-Fei Song^{*a}

^aState Key Laboratory of Chemical Resource Engineering, Beijing Advanced Innovation Center for Soft Matter Science and Engineering, Beijing University of Chemical Technology, Beijing 100029 P. R. China.

*E-mail: songyufei@hotmail.com or songyf@mail.buct.edu.cn; Tel/Fax: +86 10-64431832.

^bWestCHEM, School of Chemistry, University of Glasgow, Glasgow G12 8QQ, U.K. *E-mail: charalampos.moiras@glasgow.ac.uk

Abstract: As a biomass-derived platform molecule, 5-hydroxymethylfurfural (5-HMF) is a highly desirable feedstock for manufacturing of high value-added chemicals ranging from starting materials for polyesters to biofuels. In this work, we reported the fabrication of a series of multicomponent solid acid catalysts based on heteropolyacids immobilized ILs-modified organosilica hollow nanospheres (denoted as PW₁₂-ILs-Cn-HNS), in which PW₁₂ (PW₁₂ = H₃PW₁₂O₄₀•xH₂O) provides Brønsted acid site, ILs show strong electrostatic interactions with PW₁₂, Cn (Cn = alkyl chain) is attached for hydrophobicity and HNS represents organosilica hollow nanospheres. When applied for catalytic dehydration of fructose to 5-HMF, the PW₁₂-ILs-C4-HNS catalyst with 15.2% PW₁₂ loading exhibited the best dehydration activity to 5-HMF with 93.7 % yield in DMSO at 100 °C in 2 h. Compared with 2D hexagonal and 3D interconnected structures, the excellent porosity properties of hollow nanospherical structure can provide a high population of the PW₁₂ sites and enough confined nanospace for the dehydration of fructose. Moreover, the PW₁₂-ILs-Cn-HNS catalyst showed excellent stability over six catalytic cycles without obvious loss of activity. Most importantly, careful identification of the observed intermediates revealed crucial information for the dehydration process of fructose to 5-HMF. As such, the proposed heterogeneous catalysts show great potential in biomass conversion processes.

Keywords: Heterogeneous catalysis, Solid acid, Biomass, 5-HMF, Confined nanospace

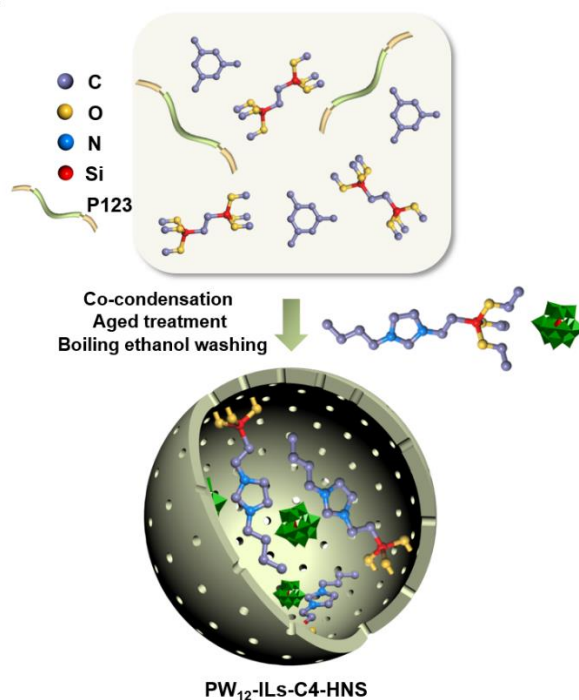
Accepted Manuscript

1. Introduction

The observed exponential growth of worldwide energy demands and concurrent depleting of fossil fuel reserves has spurred worldwide research efforts towards the energy effective and environmentally friendly production of chemicals. According to the U.S. Department of Energy^[1–3], 5-hydroxymethylfurfural (5-HMF) is one of the top 10 most valuable biomass-derived feedstocks, and is used as a versatile intermediate for the synthesis of a wide range of value-added compounds such as 2,5-furandicarboxylic acid, 2,5-dimethylfuran, 2,5-hydroxymethyl-furan, levulinic acid, caprolactam and caprolactone^[4–10]. Generally, various polysaccharides and monosaccharides are used as the starting materials^[11,12] for the synthesis of 5-HMF. Environmental and safety considerations highlight the requirement of replacing the mineral acids by environmentally-benign solid acid catalysts. To date, considerable research efforts were focused on the modification of various solid acids such as zeolites^[13–15], heteropolyacids^[15,16], sulfonated zirconia^[17,18], phosphates^[19], metal oxides^[20–23] and ion exchange resins^[15,24,25]. For the above-mentioned catalysts, the dehydration reaction required high temperature and pressure regimes or involved microwave-assisted treatment, leading to low stability, poor selectivity and leaching of the catalytically active component. As a matter of fact, an ideal catalytic system should possess a series of optimum parameters such as suitable acidic centers, hydrophobic surface and excellent catalytic stability *etc.* In addition, the effects of side reactions can be limited if the catalytic conversions take place in the confined spaces.

Heteropolyacids are widely used in catalysis^[26,27], energy storage^[28,29], and materials chemistry.^[30,31] Additionally, the heteropolyacids represent a class of green alternatives to traditional mineral acids due to their strong Brønsted acidic nature, high proton mobility and stability^[32]. However, the broad utilization of heteropolyacids is still hampered due to their low BET surface areas (1–10 m² g⁻¹) and tendency to dissolve in the reaction mixture which makes the separation process highly challenging^[33]. A simple strategy to overcome the above limitation is the immobilization of the catalytically active component on various supports, such as silica-based ones that show diverse compositions, unique structures and high surface area^[34–36].

Herein, we reported the preparation of a series of heterogeneous catalysts by immobilizing heteropolyacids within the confined space of the ILs-modified organosilica hollow nanospheres (denoted as PW₁₂-ILs-Cn-HNS). The as-prepared PW₁₂-ILs-Cn-HNS exhibited much higher catalytic activity compared with commercially available acid catalysts, such as Amberlyst-15 *etc.*, and in some cases even higher than the homogeneous system based on H₃PW₁₂O₄₀ under the same reaction conditions.



Scheme 1. Illustration of the employed synthetic procedure for the preparation of heteropolyacids immobilized on ILs-modified organosilica hollow nanospheres by taking PW₁₂-ILs-C4-HNS as an example.

2. Experimental

2.1 Chemicals and materials

All chemicals were of analytical grade and were used as received without any further purification. Pluronic P123 (EO₂₀PO₇₀EO₂₀, $M_w = 5800$) was purchased from Sigma-Aldrich; 1,2-bis(trimethoxysilyl)ethane (BTMSE, 97%), fructose and 5-HMF were purchased from Energy Chemicals; HCl, 1,3,5-trimethylbenzene (TMB), phosphotungstic acid (H₃PW₁₂O₄₀), silicotungstic acid (H₄SiW₁₂O₄₀), phosphomolybdic acid (H₅PMo₁₂O₄₀) and silicomolybdic acid (H₄SiMo₁₂O₄₀) were purchased from Beijing Chemical Company. 1-butyl-3-(3-triethoxysilylpropyl)-4,5-dihydroimidazolium hexafluorophosphate ((EtO)₃Si-ILs-C4), 1-octyl-3-(3-triethoxy-silylpropyl)-4,5-dihydroimidazolium hexafluorophosphate ((EtO)₃Si-ILs-C8), and 1-dodecyl-3-(3-triethoxy-silylpropyl)-4,5-dihydroimidazolium hexafluorophosphate ((EtO)₃Si-ILs-C12) were synthesized and characterized according to literature method^[37].

2.2 Catalyst synthesis

PW₁₂-ILs-Cn-HNS. Typically, P123 (0.5 g, 0.086 mmol) was dissolved in a mixture of water (12.7 mL), HCl (12 mol L⁻¹, 2.4 mL, 28.8 mmol) and TMB (1.3 mL, 9.02 mmol) under stirring at room temperature for 1 h. Subsequently, BTMSE (0.6 mL, 2.34 mmol), (EtO)₃Si-ILs-Cn (n = 4, 8 and 12, 0.21–0.27 g) and H₃PW₁₂O₄₀ (0.75 g, 0.26 mmol) were added successively to the above solution at the interval of every 1 h. The molar ratio of the starting materials was P123 : H₂O : HCl : TMB : BTMSE : ILs-Cn : H₃PW₁₂O₄₀ = 0.86 : 7056 : 248 :

90.23 : 23.37 : 5.12 (or 5.15 or 5.17) : 2.60. The resulting suspension was stirred at 40 °C for 24 h, and then aged at 100 °C for additional 24 h. Subsequently, the formed products were dried at 100 °C overnight and washed with boiling ethanol to remove the P123. Finally, these products were dried at 100 °C in air for 12 h (denoted as PW₁₂-ILs-Cn-HNS).

SiW₁₂-ILs-Cn-HNS, PMo₁₂-ILs-Cn-HNS, SiMo₁₂-ILs-Cn-HNS were prepared in a similar procedure as in the case of PW₁₂-ILs-Cn-HNS except that H₄SiW₁₂O₄₀, H₅PMo₁₂O₄₀, H₄SiMo₁₂O₄₀ were used instead of H₃PW₁₂O₄₀.

PW₁₂-ILs-Cn-2D_{hex} (2D_{hex} = two dimensional hexagonal nanostructure), **PW₁₂-ILs-Cn-3D_{int}** (3D_{int} = three dimensional interconnected nanostructure) were prepared following a similar procedure as in the case of PW₁₂-ILs-Cn-HNS apart from the relevant initial ratios of the reagents. The initial molar ratio used in the case of PW₁₂-ILs-Cn 2D_{hex} was P123 : H₂O : HCl : BTMSE : ILs-Cn : H₃PW₁₂O₄₀ = 0.86 : 7056 : 83.76 : 23.37 : 5.12 : 2.60. The initial molar ratio of PW₁₂-ILs-Cn 3D_{int} was P123 : H₂O : HCl : BTMSE : ILs-Cn : H₃PW₁₂O₄₀ = 0.43 : 7056 : 164.73 : 23.37 : 5.12 : 2.60.

2.3 Catalyst characterization

The N₂ adsorption-desorption measurements were performed on a Micromeritics ASAP 2020M surface area and porosity analyzer after the samples were degassed under vacuum at 363 K for 1 h and at 373 K for additional 12 h. High-resolution transmission electron microscopy (HRTEM) observations were performed on a JEM-2100 at an accelerating voltage of 400 kV. ¹³C cross polarization-magic angle spinning (CP-MAS) NMR, ³¹P and ²⁹Si MAS NMR spectra were recorded on a Bruker AV400 NMR spectrometer equipped with a 4 mm standard bore CP MAS probe head. The dried and finely powdered samples were packed in the ZrO₂ rotor closed with Ke-F cap which were spun at 12 KHz rate. Chemical shifts for all ³¹P MAS NMR, ¹³C CP-MAS NMR and ²⁹Si MAS NMR spectra were referenced to the signal of NH₄H₂PO₄ (δ = 0.00), C₁₀H₁₆ (δCH₂ = 38.5) and 3-(trimethylsilyl)-1-propanesulfonic acid sodium salt (δ = 0.0), internal standard respectively. PW₁₂ loading was determined using a Shimadzu ICPS-7500 instrument. X-ray photoelectron spectroscopy (XPS) measurements were performed using monochromatized ALK exciting X-radiation (PHI Quantera SXM). Thermogravimetric (TG) analysis was conducted on a STA-449C Jupiter equipment (HCT-2 Corporation, China) using a heating rate of 10 °C min⁻¹ in the range of 25 to 800 °C under air atmosphere. Fourier transform infrared (FTIR) spectra were recorded on a Bruker Vector 22 infrared spectrometer using the KBr pellet method.

The Brönsted acid density of the prepared catalysts was measured by acid-base titration. The fresh sample (60 mg) was suspended in deionized water (15 mL) stirred at 30 °C for 24 h. Subsequently, the suspension was cooled down to room temperature, and then it was titrated

with NaOH solution (4.0 mmol L⁻¹) that was titrated with standard potassium hydrogen phthalate solution (4.5 mmol L⁻¹). The acid densities of the prepared catalysts were determined based on the amount of consumed sodium hydroxide, and they were expressed by the number of equivalents of H⁺ ($A_{\text{titration}}, \mu\text{eq}(\text{H}^+) \text{g}^{-1}$). The Brønsted acid strength was measured by an automatic potentiometric titration system based on the literature method^[38,39]. The sample (0.050 g) was dispersed in acetonitrile and stirred for 12 h, and the resulting suspension was titrated with a solution of *n*-butylamine in acetonitrile (0.1 mol L⁻¹).

2.4 Catalytic tests

The catalysts were dried at 120 °C for 2 h before the catalytic tests. Typically, dehydration of fructose to produce 5-HMF was performed under the conditions of 0.25 mol L⁻¹ fructose in dimethylsulfoxide (DMSO), 60 mg catalysts at 100 °C. After completion of the reaction, 50 μL of the reaction mixture was withdrawn, diluted with 6 mL methanol, filtered using PTEE 0.2 μm filters and analyzed using an Agilent Technologies 1200HPLC. The concentration of fructose and the resultant 5-HMF were quantified using an Agilent Hi-Plex Ca column (film thickness 8 μm, *i.d.* 7.7 mm, length 300 mm) at 80 °C, refractive index detector and Agilent C18 column (film thickness 1.8 μm, *i.d.* 4.6 mm, length 50 mm) at 35 °C and UV detector, respectively. The catalytic activity was evaluated by determining the yield of 5-HMF ($Y, \%$), where $Y(\%) = (M_D/M_T) \times 100$ where M_D, M_T represent the number of moles of 5-HMF produced and theoretically calculated. The conversion of fructose ($C, \%$) was calculated using the formula $C(\%) = (M_{\text{initial}} - M_t/M_{\text{initial}}) \times 100$, where M_{initial} and M_t represented the number of moles of fructose at initial time ($t = 0$) and time t , respectively. The possible intermediates and byproducts yielded during the process of fructose dehydration were identified by Waters Quattro Premier XE mass spectrometry.

3 Results and discussion

3.1 Preparation and characterization of the PW₁₂-ILs-Cn-HNS nanospheres

The PW₁₂-ILs-Cn-HNS nanospheres were prepared using a P123-directed sol-gel route. The process involved hydrolysis and condensation of the BTMSE and ionic liquid (EtO)₃Si-ILs-Cn ($n = 4, 8$ and 12) in the presence of TMB under acidic conditions assisted by the electrostatic interactions developed between ILs-Cn with H₃PW₁₂O₄₀ (Scheme 1). The molar ratio of the initial materials (P123 : H₂O : HCl : TMB : BTMSE : ILs-Cn : H₃PW₁₂O₄₀) was crucial for preparation of the hollow nanospheres. It was identified that the relevant ratio of the components should be carefully adjusted to the above optimum values since they affect dramatically the rates of hydrolysis, condensation of silica precursors, the morphologies of lyotropic liquid crystal phases. The next step involved addition of H₃PW₁₂O₄₀ anions to the ILs-modified silica/carbon framework, resulting in the formation of the PW₁₂-ILs-Cn-HNS

composite. The aging of the above mixture at 100 °C for 24 h was crucial for efficient interaction of the ILs-Cn and $\text{H}_3\text{PW}_{12}\text{O}_{40}$ anions. Finally, the $\text{PW}_{12}\text{-ILs-Cn-HNS}$ with hollow spherical nanospheres morphologies can be achieved after removal of P123 by washing with boiling ethanol.

In contrast to the post-grafting synthetic method with multiple step process and/or the impregnation method with poor dispersion of the active sites, the sol-gel strategy not only is facile and time-saving, but also leads to the $\text{PW}_{12}\text{-ILs-Cn-HNS}$ with well-defined mesoporosity, uniform dispersion and controllable loadings of catalytically active sites. Different alkyl chains can be incorporated into the $\text{PW}_{12}\text{-ILs-Cn-HNS}$ by simply adjusting the corresponding $(\text{EtO})_3\text{Si-ILs-Cn}$, demonstrating the modularity of this approach. Another noteworthy feature is the ability of the amphiphilic triblock copolymer, *i.e.*, Pluronic P123, can be assembled into micelles through hydrogen bonding and/or hydrophobic/hydrophilic interactions in acidic media due to the presence of both hydrophilic $-\text{CH}_2\text{CH}_2\text{O}$ (PEO) and hydrophobic $-\text{CH}_2(\text{CH}_3)\text{CHO}$ (PPO) groups. Initially, the PPO blocks form the core of the spherical micelles, while the PEO blocks form a hydrated corona around the core, followed by the expansion of the micelles driven by the diffusion of the swelling agent (TMB) into the core of the nanostructure. The surface charge density on micelles gradually decreases as a function of the TMB molecules that diffuse into the micelles, leading to the formation of well-defined and stable hollow spherical nanostructures.

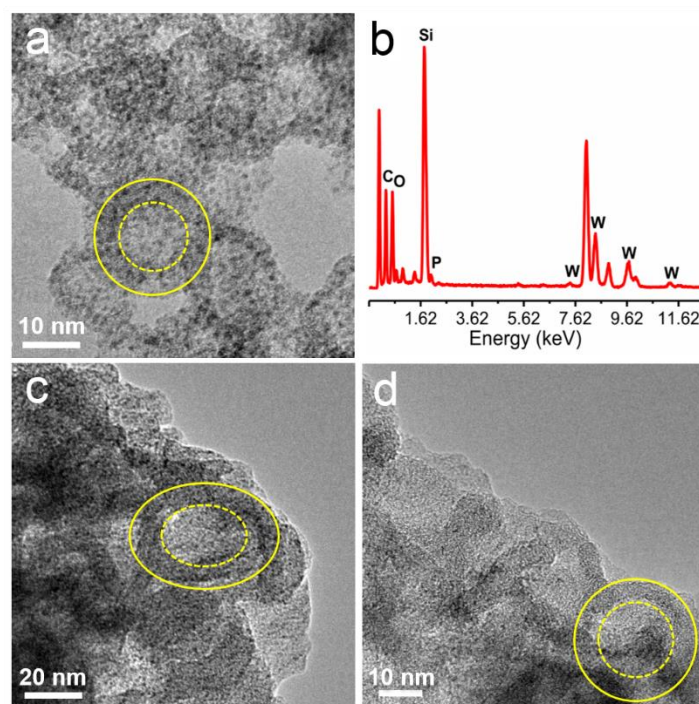


Fig. 1 HRTEM images of (a) $\text{PW}_{12}\text{-ILs-C4-HNS}$; (c) $\text{PW}_{12}\text{-ILs-C8-HNS}$; (d) $\text{PW}_{12}\text{-ILs-C12-HNS}$; (b) EDX of $\text{PW}_{12}\text{-ILs-C4-HNS}$.

Morphological characteristics and textural properties. Fig. 1 presents HRTEM images of three $\text{PW}_{12}\text{-ILs-Cn-HNS}$ nanospheres, which are all composed of small and uniform spherical nanostructures with hollow interior. Close inspection of the images shows that the prepared $\text{PW}_{12}\text{-ILs-C4-HNS}$ nanospheres are well-defined with uniformly dispersed black spots of 1–1.5 nm in diameter. This is in agreement with the dimensions of the $\text{H}_3\text{PW}_{12}\text{O}_{40}$ clusters, and suggests that the active sites (*i.e.*, $\text{H}_3\text{PW}_{12}\text{O}_{40}$) are uniformly incorporated into the silica/carbon framework.

In terms of $\text{PW}_{12}\text{-ILs-C8-HNS}$ (Fig. 1c) and $\text{PW}_{12}\text{-ILs-C12-HNS}$ (Fig. 1d), they both form nanospheres with uniform morphology. The energy-dispersive X-ray spectrometry of $\text{PW}_{12}\text{-ILs-C4-HNS}$ (Fig. 1b) reveals the presence of C, O, Si, P and W elements, which is consistent with the composition of the nanospheres.

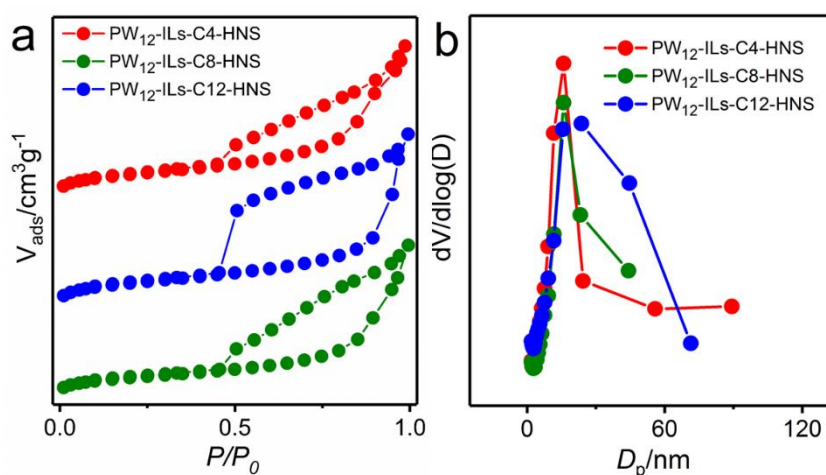


Fig. 2 The N_2 adsorption-desorption isotherms (a) and BJH pore size distribution profiles (b) of various $\text{PW}_{12}\text{-ILs-Cn-HNS}$ ($n = 4, 8, \text{ and } 12$; POM loading: 15.2%).

Fig. 2a shows the N_2 adsorption-desorption isotherms, in which the type IV isotherms confirm the mesoporous nature of the $\text{PW}_{12}\text{-ILs-Cn-HNS}$. Moreover, they all exhibit one hysteresis loop that can be attributed to the hollow interior of the spherical nanostructures or the void space formed between the loosely packed spheres^[40,41]. The capillary condensation steps occur at $P/P_0 = 0.45\text{--}0.99$. In addition, with increasing of the PW_{12} loading from 5.8, 8.7 to 17.6, the hysteresis loop becomes smaller accordingly (Fig. S3a).

As shown in Fig 2b, BJH pore size distribution curves show that the $\text{PW}_{12}\text{-ILs-C4-HNS}$, $\text{PW}_{12}\text{-ILs-C8-HNS}$ and $\text{PW}_{12}\text{-ILs-C12-HNS}$ exhibit one peak at 15.7, 15.3 and 15.6 nm, respectively, which confirms the mesoporous structure of the nanospheres and corresponds to the uniform hollow interior of the nanospheres. As shown in Table 1, the $\text{PW}_{12}\text{-ILs-Cn-HNS}$ nanospheres exhibit a large BET surface area ($125\text{--}156\text{ m}^2\text{ g}^{-1}$) and high pore volume ($0.40\text{--}0.47\text{ cm}^3\text{ g}^{-1}$). Moreover, the length of alkyl-chain does not affect dramatically on the porosity of the produced catalyst.

Table 1 The physical-chemical parameters of various heteropolyacids immobilized on ionic liquids-modified organosilica nanospheres and reference catalysts.

Catalysts	S_{BET} ($\text{m}^2 \text{g}^{-1}$) ^a	D_{p} (nm) ^b	V_{p} ($\text{cm}^3 \text{g}^{-1}$) ^c	$A_{\text{titration}}$ ($\mu\text{eq g}^{-1}$) ^d	E_{i} (mV) ^e
PW ₁₂ -ILs-C4-HNS	140	15.7	0.43	1179	596.7
PW ₁₂ -ILs-C8-HNS	156	15.3	0.40	987	557.4
PW ₁₂ -ILs-C12-HNS	125	15.6	0.47	860	456.2
Amberlyst-15	50 ^f	n.d.	n.d.	4800 ^f	470.7 ^g
H ₃ PW ₁₂ O ₄₀	5.0 ^h	n.d.	n.d.	3000	720.2

Note: POM loading is 15.2%; ^a Surface area (S_{BET}) was calculated using Brunauer–Emmett–Teller (BET) equation. ^b Pore diameter (D_{p}) was estimated from BJH adsorption determination. ^c Pore volume (V_{p}) was estimated from the pore volume determination using the adsorption branch of the N₂ isotherm curve at $P/P_0 = 0.99$ single point. ^d Acid density (A) was measured by acid-base titration. ^e Initial electrode potential (E_{i}) was determined by nonaqueous potentiometric titration with *n*-butylamine in acetonitrile (0.1 mol L⁻¹). ^f The data were cited from Ref. [42]. ^g The data was cited from Ref. [43]. ^h The data was cited from Ref. [44].

The structural integrity of the as-prepared PW₁₂-ILs-Cn-HNS nanospheres were confirmed by FT-IR (Fig. 3a), W 4f XPS (Fig. 3b), ³¹P (Fig. 3c) and ²⁹Si MAS NMR (Fig. 3d).

FT-IR of H₃PW₁₂O₄₀ shows characteristic vibration peaks centered at 1079, 985, 890 and 795 cm⁻¹, respectively, which can be assigned to the stretching of tetrahedral P–O bonds, terminal W=O_t bonds and two types of bending vibrations originating from the bridging W–O_b–W bonds. The above four characteristic vibrational signals can be observed in the FT-IR spectra of PW₁₂-ILs-C4-HNS, PW₁₂-ILs-C8-HNS and PW₁₂-ILs-C12-HNS. Furthermore, the stretching bands located at 1658 and 2932 cm⁻¹ originate from the presence of –CH₂ or –CH₃ and C=N groups of ILs, respectively. These results indicate that 1) the as-prepared ionic liquid and PW₁₂ were successfully incorporated into the hollow nanospheres; 2) the primary Keggin structure remained intact after immobilization, regardless the length of the carbon-chain.

As shown in Fig. 3b, the W 4f XPS spectrum of the PW₁₂-ILs-C4-HNS hollow nanospheres is deconvoluted into two signals centered at 38.4 and 36.3 eV due to the W 4f_{5/2} and W 4f_{7/2} spin-orbit components accordingly. As can be seen from the ³¹P MAS NMR spectroscopy in Fig. 3c, the sharp peak centered at -15.2 ppm can be assigned to the resonance of the encapsulated PO₄³⁻ units within the H₃PW₁₂O₄₀ cage, indicating the structural integrity of the incorporated H₃PW₁₂O₄₀.

In a similar manner, the ²⁹Si MAS NMR spectra reveal characteristic resonance peaks centered at -66.0, -63.6 and -64.3 ppm for the PW₁₂-ILs-C4-HNS, PW₁₂-ILs-C8-HNS and PW₁₂-ILs-C12-HNS, respectively, which can be attributed to the organosiloxane species of T³ [-CH₂CH₂Si(OSi)₃] within the ethyl-bridged organosilica framework and covalently tethered ILs (Fig. 3d). Most importantly, the absence of resonance signals corresponding to the inorganic

Si-containing starting materials, such as Q^3 [$Si(OSi)_3(OH)$, $\delta = -90$ ppm] and Q^4 [$Si(OSi)_4$, $\delta = -120$ ppm]^[45,46] provides additional evidence for the successful formation of the IL functionalized ethyl-bridged organosilica structures.

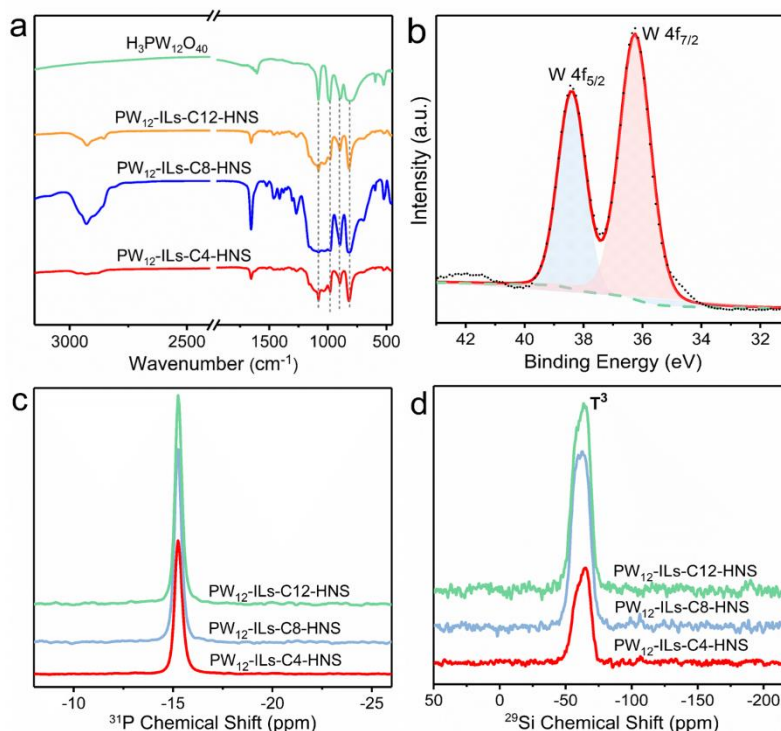


Fig. 3 (a) Characteristic FT-IR fingerprint region of the incorporated heteropolyacid on the ILs-modified organosilica nanospheres; (b) XPS spectrum of the W $4f$ core level of PW_{12} -ILs-C4-HNS; (c) ^{31}P and (d) ^{29}Si MAS NMR spectra of the PW_{12} -ILs-C4-HNS, PW_{12} -ILs-C8-HNS and PW_{12} -ILs-C12-HNS.

The Brønsted acid densities of the PW_{12} -ILs-C n -HNS nanospheres were determined by acid-base titration using NaOH solution (4.0 mmol L^{-1}). As shown in Table 1, PW_{12} -ILs-C n -HNS ($n = 4, 8$ and 12) with different alkyl-chain length exhibit comparable Brønsted acid density of 860, 987 and $1179 \mu\text{eq}(\text{H}^+) \text{g}^{-1}$, respectively.

The thermogravimetric studies were carried out in the range of 30 to 800 °C. As shown in Fig. S4, the TGA of PW_{12} -ILs-C4-HNS composite shows three consecutive weight losses. The first weight loss occurs in the range of 30 to 100 °C (*ca.* 1.6%) which can be attributed to the loss of water molecules adsorbed by the nanospheres. The second weight loss in the range of 200 to 500 °C (*ca.* 14.1%) can be attributed to the decomposition of the bridging ethyl groups, ionic liquid and residual P123. The third one takes place in the range of 400 to 800 °C (*ca.* 3.6%), which can be due to the elimination of the silica/carbon framework's carbon content before the collapse of the framework and decomposition of the Keggin structure. As a consequence, the prepared PW_{12} -ILs-C n -HNS nanospheres are thermally stable up to 200 °C.

3.2 Catalytic studies

In order to optimize the heteropolyacids immobilized on ILs-modified organosilica hollow

nanospheres, the influences of the composition and loading of heteropolyacids as well as the alkyl-chain length on the catalytic activity were carefully investigated under the conditions of 100 °C and 0.25 mol L⁻¹ fructose in DMSO for 2 h.

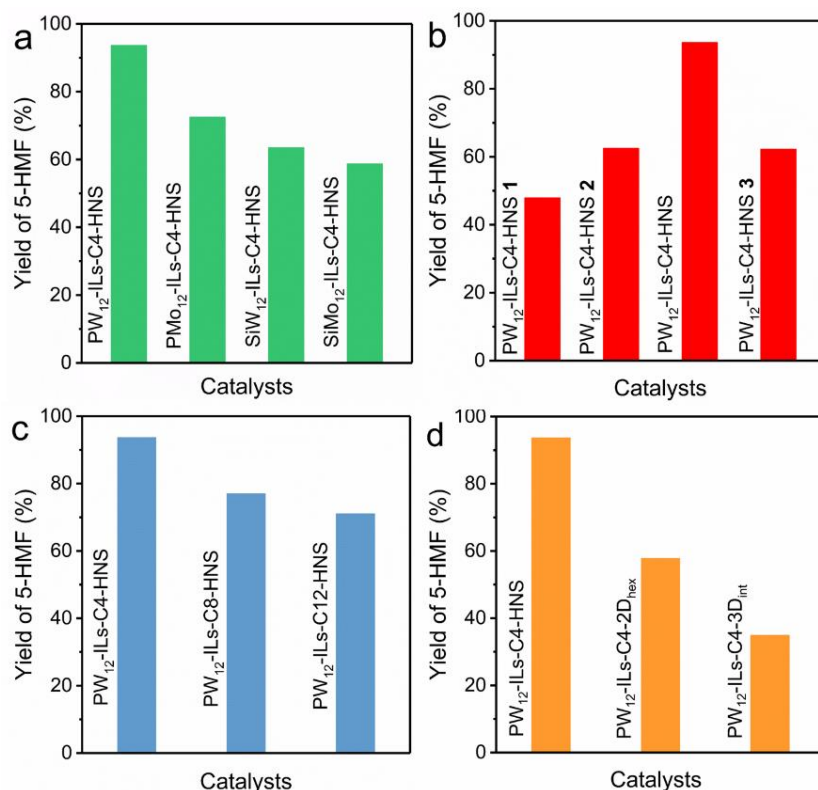


Fig. 4 Influence of the (a) heteropolyacids, (b) PW₁₂ loading, (c) ionic liquid with different alkyl-chain length and (d) morphological nanostructure on the catalytic activity of the catalysts. Reaction conditions: 0.25 mol L⁻¹ fructose in DMSO, 60 mg catalyst.

As shown in Figure 4a, the dehydration activity of a series of catalysts incorporating different heteropolyacids followed this sequence of PW₁₂-ILs-C4-HNS > PMo₁₂-ILs-C4-HNS > SiW₁₂-ILs-C4-HNS > SiMo₁₂-ILs-C4-HNS, while the corresponding 5-HMF yield can be found to be 93.7, 72.5, 63.5 and 58.7%, respectively. Moreover, the PW₁₂-ILs-C4-HNS exhibited the best activity that can be attributed to the fact that the H₃PW₁₂O₄₀ possess the strongest Brönsted acid strength among the selective heteropolyacids, which promote the release of protons during the dehydration of fructose.

The influence of PW₁₂ loading on the dehydration activity was evaluated. Our observations are summarized in Fig. 4b, where the yield of 5-HMF continuously increases from 47.9, 62.5 to 93.7 after 2 h with increasing the PW₁₂ loading (5.8, 8.7 to 15.2 %). However, the yield drops abruptly to 62.2% upon further increase of the PW₁₂ loading. Further increase of the PW₁₂ loading leads to undesirable blocking of the pores of the prepared PW₁₂-ILs-C4-HNS nanospheres, and consequently to decreased 5-HMF yield. Therefore, the optimum PW₁₂ loading of 15.2 was used for subsequent catalytic tests.

Then, the dehydration activity using catalysts with different alkyl-chains on ionic liquids were tested (Fig. 4c). The catalytic activity decreases as the following sequence $PW_{12}\text{-ILs-C4-HNS} > PW_{12}\text{-ILs-C8-HNS} > PW_{12}\text{-ILs-C12-HNS}$ with the 5-HMF yields of 93.7, 77.0 and 71.1%, respectively. This result indicates that the dehydration activity is influenced by the hydrophobicity microenvironment of ILs-modified organosilica particles. The composition of $PW_{12}\text{-ILs-C4-HNS}$ catalyst proved to be a fine balance of the various parameters that affect the catalytic process and showed the best activity, which leads to efficient mass transfer of fructose molecules to the active sites and higher dehydration activity.

The influence of the morphological nanostructures on dehydration activity was investigated (Fig. 4d). The order was as following $PW_{12}\text{-ILs-C4-HNS} > PW_{12}\text{-ILs-C4-2D}_{\text{hex}} > PW_{12}\text{-ILs-C4-3D}_{\text{int}}$, and the corresponding 5-HMF yield was found to be 93.7, 57.8 and 34.9%, respectively. In comparison with $PW_{12}\text{-ILs-C4-2D}_{\text{hex}}$ with hexagonal nanostructure (Fig. S1a) and $PW_{12}\text{-ILs-C4-3D}_{\text{int}}$ (Fig. S1b) with interconnected nanostructure, the $PW_{12}\text{-ILs-C4-HNS}$ with unique hollow spherical nanostructure exhibited higher activity due to the short diffusion pathway.

In addition, we investigated carefully the influence of temperature, reaction time and solvents on 5-HMF yield by taking the optimized $PW_{12}\text{-ILs-C4-HNS}$ as the representative catalyst.

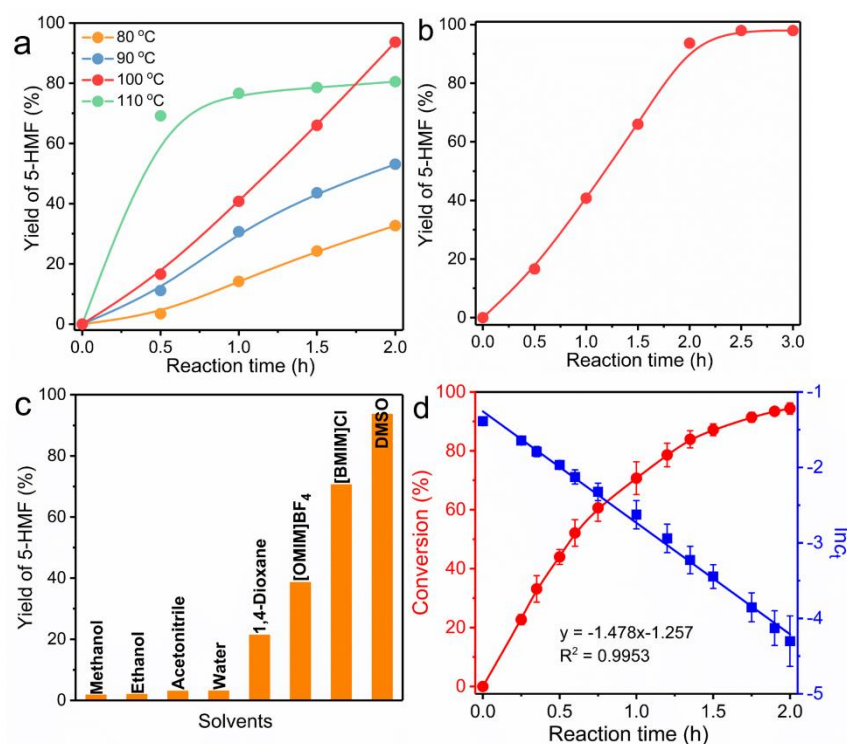


Fig. 5 Influence of the (a) temperature, (b) reaction time, and (c) solvents on the catalytic activity of the $PW_{12}\text{-ILs-C4-HNS}$. Reaction conditions: 0.25 mol L⁻¹ fructose in solvent (methanol, ethanol, acetonitrile, water, 1,4-dioxane or DMSO) or 90 mg fructose in 1 g [BMIM]Cl or [OMIM]BF₄; 60 mg catalyst. (d) Kinetic

profiles of the dehydration. Reaction conditions: 0.25 mol L⁻¹ fructose in DMSO, 60 mg catalyst.

As shown in Fig. 5a, the yield of 5-HMF continuously increases from 32.7, 53.1 to 93.7% with increasing the reaction temperature from 80, 90 to 100 °C. Further increase of the temperature to 110 °C leads to the formation of 5-HMF rapidly with a yield of 69.2% in the first 30 min. After that, the dehydration reaction rate becomes slower gradually, before reaching the yield of 80.5% after prolonging the reaction time to 2 h. Thus, the optimum reaction temperature for this catalytic system determined to be 100 °C.

The reaction time was investigated by proceeding the dehydration reaction for 3 h (Fig. 5b). The results show that the 5-HMF yield gradually increased in 2 h. With prolonging the reaction time to 2.5 h and 3 h, no obvious increase of 5-HMF can be observed. Therefore, 2 h proved to be the optimum reaction time for the efficient production of 5-HMF.

In general, the dehydration of fructose to 5-HMF in acidic media is accompanied by the formation of oligomeric byproducts or formic acid, which is detrimental on the selectivity. Thus, the effect of solvents (methanol, ethanol, acetonitrile, water, 1,4-dioxane, [BMIM]Cl, [OMIM]BF₄ and DMSO) on the dehydration process was carried out^[47,48]. As shown in Fig. 5c, methanol, ethanol, acetonitrile and water exhibit similar dehydration activity and a yield of 1.8, 2.0, 3.1 and 3.1 %, respectively, after 2 h. Under the same conditions, 1, 4-dioxane shows slightly increased dehydration activity and a yield of 21.4%. In contrast, the yields of 38.6% and 70.6% were obtained by using the [OMIM]BF₄ and [BMIM]Cl as solvents, respectively. The highest dehydration activity was achieved when the catalytic reaction carried out in DMSO where the yield reached the value of 93.7 % over a period of 2 h. The DMSO, not only inhibits any side-reactions which lead to the formation of furanoid^[49], but also interacts with H⁺ to form [DMSOH]⁺ cations^[3,50]. As such, DMSO was selected as solvent for the subsequent catalytic tests.

To obtain the kinetic parameters for the PW₁₂-ILs-C4-HNS-catalyzed dehydration of fructose, conversion of fructose and $\ln c_t$ was plotted against the reaction time (Fig. 5d), in which c_t represented the fructose concentration at time t . The linear fit of the data revealed that the PW₁₂-ILs-C4-HNS-catalyzed dehydration reaction shows first-order kinetics ($R^2 = 0.9953$).

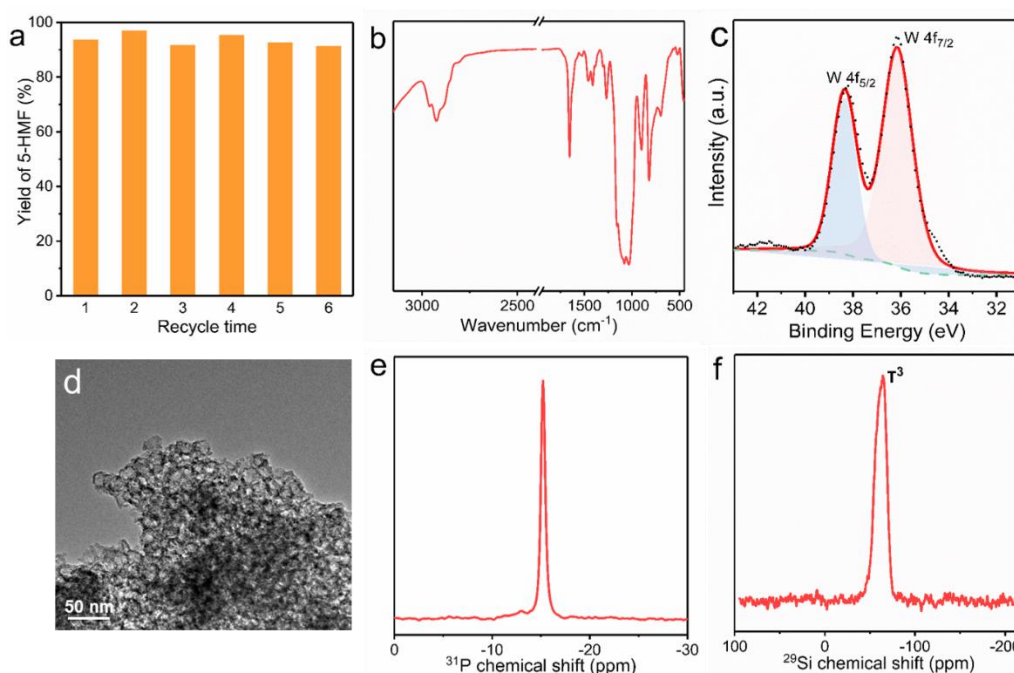


Fig. 6 Reusability of the $\text{PW}_{12}\text{-ILs-C4-HNS}$ in dehydration reaction (a) and FT-IR spectrum (b), W $4f$ core level (c), TEM image (d), ^{31}P (e) and ^{29}Si (f) MAS NMR of the used $\text{PW}_{12}\text{-ILs-C4-HNS}$ nanospheres.

Regeneration and reusability. Large scale applications and continuous manufacturing processes require the use of catalytic systems which can be easily recycled and reused for prolonged period of times. To evaluate the reusability and stability of the catalytic system, the $\text{PW}_{12}\text{-ILs-C4-HNS}$ catalyst catalyzed the dehydration of fructose for six consecutive cycles under the optimized reaction condition. After each catalytic cycle, the catalyst was removed by filtration, washed with ethanol and acetone before the next cycles. As shown in Fig. 6a, the yields of 5-HMF are found to be 93.7, 96.9, 91.7, 95.2, 92.6 and 91.2%, respectively, for the consecutive catalytic cycles. In order to identify potential leaching of the $\text{H}_3\text{PW}_{12}\text{O}_{40}$ species into the solution, we conducted ICP-AES analyses to determine the tungsten content in the reaction mixture after removing the catalyst at the end of the cycle. The results showed that the concentration of the tungsten in the system is below the detection limit confirming that there is no detectable leaching of $\text{H}_3\text{PW}_{12}\text{O}_{40}$ species under the experimental conditions. Subsequently, the structure of the recycled $\text{PW}_{12}\text{-ILs-C4-HNS}$ catalyst was further evaluated by FT-IR, XPS, ^{31}P and ^{29}Si MAS NMR. Fig. 6b shows the FT-IR characteristic peaks which can still be detected and assigned to the Keggin and ILs species. The deconvoluted W $4f$ XPS spectrum reveals again in this case two signals centered at 38.4 and 36.3 eV (Fig. 6c), originating from the contributions of the W $4f_{5/2}$ and W $4f_{7/2}$ spin-orbit components, which found to be identical to the freshly prepared $\text{PW}_{12}\text{-ILs-C4-HNS}$ catalyst. Additionally, TEM image in Fig. 6d shows well-dispersed hollow nanospheres, which indicates that the confined nanostructure of as-prepared catalysts was retained after recycling. Subsequently, the peaks centered at -15.2 and -

64.5 ppm in ^{31}P and ^{29}Si MAS NMR spectra (Figs. 6e and f), confirms that the $\text{H}_3\text{PW}_{12}\text{O}_{40}$ species retain their structural integrity after the catalytic cycle. Based on the above observations, we can conclude that the prepared $\text{PW}_{12}\text{-ILs-Cn-HNS}$ nanospheres can act as efficient and stable solid acid catalysts for the dehydration reaction of fructose.

Comparison with the reference solid acids. The prepared $\text{PW}_{12}\text{-ILs-C4-HNS}$ catalyst was further compared with the $\text{H}_3\text{PW}_{12}\text{O}_{40}$ and Amberlyst-15 under the same reaction condition. As shown in Table 2, $\text{PW}_{12}\text{-ILs-C4-HNS}$ -catalyzed dehydration reaction of fructose exhibits a yield of 93.7% which is in marked contrast to the yields observed in the case of Amberlyst-15 and $\text{H}_3\text{PW}_{12}\text{O}_{40}$ catalysts with yields of 63.1 and 58.4%, respectively. This is due to the fact that the strong Brønsted acidity of $\text{H}_3\text{PW}_{12}\text{O}_{40}$ and Amberlyst-15 facilitates simultaneously the occurrence of side-reactions, which leads to poor selectivity for 5-HMF. In marked contrast, the $\text{PW}_{12}\text{-ILs-C4-HNS}$ exhibits the acid density of $1179 \mu\text{eq g}^{-1}$ and E_i of 596.7 mV which leads ultimately to the efficient dehydration activity without promotion of side-reactions, and a high yield of 93.7% over 2 h. Moreover, the dehydration activity of $\text{PW}_{12}\text{-ILs-C4-HNS}$ catalyst was further compared to the other reported examples. The results in Table 2 confirm that the prepared $\text{PW}_{12}\text{-ILs-C4-HNS}$ catalyst could work efficiently in the dehydration of fructose under mild reaction conditions.

Table 2 Dehydration activity comparison of $\text{PW}_{12}\text{-ILs-C4-HNS}$ with the reference solid acids.

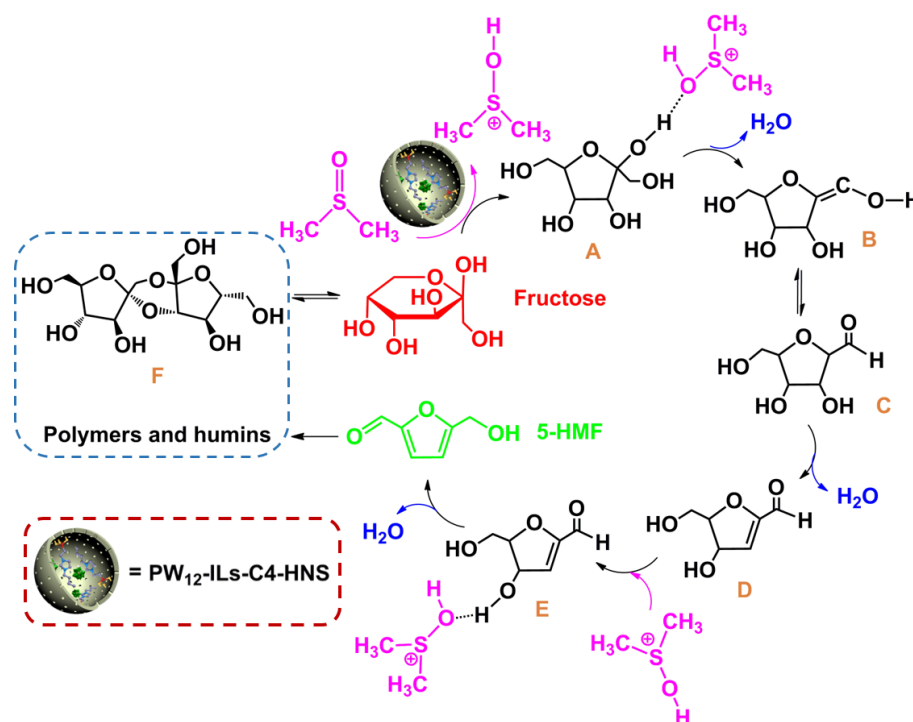
Catalysts	T (°C)	Solvent	T (min)	Yield (%)	Reference
$\text{PW}_{12}\text{-ILs-C4-HNS}$	100	DMSO	120	93.7	This work
Amberlyst-15	100	DMSO	120	63.1	This work
$\text{H}_3\text{PW}_{12}\text{O}_{40}$	100	DMSO	120	58.4	This work
SPAN-11/3	140	Water/1,4-Dioxane	180	71	Ref 51
TESAS-SBA-15	130	MIBK/2-Butanol	141	59.6	Ref 52

Note: TEASA is 3-((3-(trimethoxysilyl)propyl)thio)propane-1-sulfonic acid and SPAN is sulfonated polyaniline.

In order to elucidate the reaction mechanism of the $\text{PW}_{12}\text{-ILs-C4-HNS}$ catalyzed dehydration of fructose, we used mass spectrometry to identify the intermediate species (Scheme 2 and Fig. S8). In the initial stage, the DMSO is protonated firstly *via* the proton transfer process^[3,50,53], and an intermediate is obtained (**A**) *via* hydrogen bonding interactions between fructose and the protonated DMSO. Then, the enol (**B**), 2,5-anhydro-D-mannose (**C**), and 4-hydroxy-5-(hydroxymethyl)-4,5-dihydrofuran-2-carbaldehyde (**D**) are successively formed, accompanied with the release of water molecules. Finally, the 5-HMF can be obtained

by releasing the water and DMSO molecules.

Importantly, the formation of the 5-HMF can potentially take place in tandem with various side-reactions. For example, the formation of byproduct of difructose anhydride (**F**) is promoted by strong acidic conditions. Consequently, the target product (5-HMF) can further transform to polymers and humins or formic and levulinic acids *via* a rehydration reaction^[54]. Based on the above observations it is concluded that the best dehydration activity of PW₁₂-ILs-C4-HNS catalyst can be attributed to its Brønsted acidity (Brønsted acid density of 1179 $\mu\text{eq g}^{-1}$ and E_i of 596.7 mV). Finally, it is worth noting that the hydrophobic surface of as-prepared PW₁₂-ILs-C4-HNS catalyst can promote the efficient removal of the water molecules produced from the catalyst's surface and accelerate the dehydration reaction.



Scheme 2 The suggested reaction mechanism of PW₁₂-ILs-C4-HNS-catalyzed dehydration of fructose towards the formation of 5-HMF.

On the other hand, the morphological characteristics and the porosity properties of the PW₁₂-ILs-C4-HNS nanospheres influence dramatically the dehydration activity. The hollow spherical nanostructures of the PW₁₂-ILs-C4-HNS catalyst can serve as nanoreactors providing well dispersed active sites within an accessible confined space. The morphology and structural features of the spherical particles provide a short diffusion pathway, which leads to efficient mass transfer and accessibility of the active sites by the substrate. Simultaneously, the unique hollow spherical nanostructures of the prepared nanocatalysts exhibit large BET surface areas (140 $\text{m}^2 \text{g}^{-1}$) and thereby well-dispersed and controlled population of the heteropolyacids. Additionally, the high pore volume (0.43 $\text{cm}^3 \text{g}^{-1}$) of the PW₁₂-ILs-C4-HNS renders the embedded within the nanosphere catalytic sites readily accessible by the reactant molecules.

Meanwhile, the hydrophobic surface of $\text{PW}_{12}\text{-ILs-C4-HNS}$ due to the alkyl groups of the ILs-modified organosilica structures, can inhibit the formation of byproducts such as formic and levulinic acids by rehydration of the desirable product, 5-HMF, by promoting its easy removal from the catalyst's surface and ensuring that the dehydration of fructose proceeds at a considerably high rate. Therefore, the synergistic effects between the $\text{PW}_{12}\text{-ILs-Cn-HNS}$ catalyst's components in the confined space of the nanosphere, suitable Brønsted acidity of the active species (PW_{12}), excellent porosity and IL-modified organosilica hydrophobic surface, are all crucial parameters for the enhancement of the dehydration process and production of 5-HMF at considerably high yield.

4. Conclusions

A new family of heterogeneous catalysts were successfully fabricated by immobilizing PW_{12} clusters within the ILs-modified organosilica hollow nanospheres ($\text{PW}_{12}\text{-ILs-Cn-HNS}$) and fully characterized, in which the PW_{12} provides Brønsted acid site, ILs bind strongly through the electrostatic interactions with PW_{12} and Cn helps to adjust the hydrophobicity. Among them, the $\text{PW}_{12}\text{-ILs-C4-HNS}$ with PW_{12} loading of 15.2% exhibited the best activity for dehydration of fructose to 5-HMF under mild conditions. Furthermore, the $\text{PW}_{12}\text{-ILs-Cn-HNS}$ composites showed excellent stability after six consecutive catalytic cycles without obvious loss of their catalytic activity. Moreover, it has been demonstrated that compared with $\text{PW}_{12}\text{-ILs-Cn-2D}_{\text{hex}}$ and $\text{PW}_{12}\text{-ILs-Cn-3D}_{\text{int}}$, the $\text{PW}_{12}\text{-ILs-Cn-HNS}$ exhibits much improved catalytic activity, indicating the advantages of the confined nanospherical structure. Careful modulation of a number of reaction parameters and identification of the intermediate species in the reaction mixture using mass spectrometry allowed us to shed light upon the mechanistic details for the dehydration processes. The design strategy presented herein may open a new pathway for further development of cost-effective and environmentally-benign catalysts for biomass conversion applications.

Acknowledgements

This research was supported by the National Nature Science Foundation of China (21625101, 21808011, 21521005), the National Key Research and Development Program of China (2017YFB0307303), the Fundamental Research Funds for the Central Universities (XK1802-6, XK1902, 12060093063), Beijing Natural Science Foundation (2182047), Postdoctoral Science Foundation of China (2018M631313). H. N. M would like to thank the University of Glasgow for supporting this work.

References

- [1] J. Howard, D. W. Rackemann, J. P. Bartley, C. Samori, W. O.S. Doherty, *ACS Sustainable Chem. Eng.* **2018**, *6*, 4531–4538.
- [2] X. G. Zhang, K. Wilson, A. F. Lee, *Chem. Rev.* **2016**, *116*, 12328–12368.
- [3] L.-K. Ren, L.-F. Zhu, T. Qi, J.-Q. Tang, H.-Q. Yang, C.-W. Hu, *ACS Catal.* **2017**, *7*, 2199–2212.
- [4] C. García-Sancho, I. Fúnez-Núñez, R. Moreno-Tost, J. Santamaría-González, E. Pérez-Inestrosa, J.L.G. Fierro, P. Maireles-Torres, *Appl. Catal. B: Environ.* **2017**, *206*, 617–625.
- [5] R.-J. van Putten, J. C. van der Waal, E. de Jong, C. B. Rasrendra, H. J. Heeres, J. G. de Vries, *Chem. Rev.* **2013**, *113*, 1499–1597.
- [6] Y. S. Qu, Q. Y. Wei, H. Q. Li, P. Oleskowicz-Popiel, C. P. Huang, J. Xu, *Bioresour. Technol.* **2014**, *162*, 358–364.
- [7] U. Tyagi, N. Anand, D. Kumar, *Bioresour. Technol.* **2018**, *267*, 326–332.
- [8] G. S. Svenningsen, R. Kumar, C. E. Wyman, P. Christopher, *ACS Catal.* **2018**, *8*, 5591–5600.
- [9] X. Q. Jia, J. P. Ma, M. Wang, H. Ma, C. Chen, J. Xu, *Green Chem.* **2016**, *18*, 974–978.
- [10] W.-J. Liu, L. Dang, Z. Xu, H.-Q. Yu, S. Jin, G. W. Huber, *ACS Catal.* **2018**, *8*, 5533–5541.
- [11] C. J. Zhou, C. Shen, K. Y. Ji, J. B. Yin, L. Du, *ACS Sustainable Chem. Eng.* **2018**, *6*, 3992–3999.
- [12] K. Li, M. M. Du, P. J. Ji, *ACS Sustainable Chem. Eng.* **2018**, *6*, 5636–5644.
- [13] V.V. Ordonsky, J. van der Schaaf, J.C. Schouten, T.A. Nijhuis, *J. Catal.* **2012**, *287*, 68–75.
- [14] Z. S. Ma, H. L. Hu, Z. Q. Sun, W. T. Fang, J. Zhang, L. F. Yang, Y. J. Zhang, L. Wang, *ChemSusChem* **2017**, *10*, 1669–1674.
- [15] K.-I. Shimizu, R. Uozumi, A. Satsuma, *Catal. Commun.* **2009**, *10*, 1849–1853.
- [16] Y. P. Xiao, Y.-F. Song, *Appl. Catal. A: Gen.* **2014**, *484*, 74–78.
- [17] E. Kılıç, S. Yılmaz, *Ind. Eng. Chem. Res.* **2015**, *54*, 5220–5225.
- [18] X. H. Qi, M. Watanabe, T. M. Aida, R. L. Smith Jr., *Catal. Commun.* **2009**, *10*, 1771–1775.
- [19] C. Carlini, P. Patrono, A. M. R. Galletti, G. Sbrana, *Appl. Catal. A: Gen.* **2004**, *275*, 111–118.
- [20] K. Nakajima, Y. Baba, R. Noma, M. Kitano, J. N. Kondo, S. Hayashi, M. Hara, *J. Am. Chem. Soc.* **2011**, *133*, 4224–4227.
- [21] M. Watanabe, Y. Aizawa, T. Iida, R. Nishimura, H. Inomata, *Appl. Catal. A: Gen.* **2005**, *295*, 150–156.
- [22] X. H. Qi, M. Watanabe, T. M. Aida, R. L. Smith Jr., *Catal. Commun.* **2008**, *9*, 2244–2249.
- [23] A. Chareonilimkun, V. Champreda, A. Shotipruk, N. Laosiripojana, *Fuel*, **2010**, *89*, 2873–2880.
- [24] H. Tang, N. Li, G. Y. Li, W. T. Wang, A. Q. Wang, Y. Cong, X. D. Wang, *ACS Sustainable Chem. Eng.* **2018**, *6*, 5645–5652.
- [25] W. Z. Li, T. W. Zhang, H. S. Xin, M. X. Su, L. L. Ma, H. Jameel, H.-M. Chang, G. Pei, *RSC Adv.* **2017**, *7*, 27682–27688.
- [26] T. F. Li, Z. L. Wang, W. Chen, H. N. Miras, Y.-F. Song, *Chem. Eur. J.*, **2017**, *23*, 1069–1077.
- [27] B. Schwarz, J. Forster, M. K. Goetz, D. Yücel, C. Berger, T. Jacob, C. Streb, *Angew. Chem. Int. Ed.* **2016**, *55*, 6329–6333.
- [28] Y. C. Ji, L. J. Huang, J. Hu, C. Streb, Y.-F. Song, *Energy Environ. Sci.* **2015**, *8*, 776–789.
- [29] J. Hu, Y. C. Ji, W. Chen, C. Streb, Y.-F. Song, *Energy Environ. Sci.* **2016**, *9*, 1095–1101.
- [30] H.-L. Li, Y.-J. Liu, J.-L. Liu, L.-J. Chen, J.-W. Zhao, G.-Y. Yang, *Chem. Eur. J.* **2017**, *23*, 2673–2689.

- [31] H. N. Miras, J. Yan, D.-L. Long, L. Cronin, *Chem. Soc. Rev.* **2012**, *41*, 7403–7430.
- [32] S. Omwoma, W. Chen, R. Tsunashima, Y.-F. Song, *Coord. Chem. Rev.* **2014**, *258–259*, 58–71.
- [33] I. Romanenko, M. Lechner, F. Wendler, C. Hörenz, C. Streb, F. H. Schacher, *J. Mater. Chem. A* **2017**, *5*, 15789–15796.
- [34] S. An, Y. N. Sun, D. Y. Song, Q. Q. Zhang, Y. H. Guo, Q. K. Shang, *J. Catal.* **2016**, *342*, 40–54.
- [35] S. An, D. Y. Song, Y. N. Sun, Q. Q. Zhang, P. P. Zhang, Y. H. Guo, *ACS Sustainable Chem. Eng.* **2018**, *6*, 3113–3123.
- [36] F. Su, Y. H. Guo, *Green Chem.* **2014**, *16*, 2934–2957.
- [37] Y. Chen, Y.-F. Song, *ChemPlusChem* **2014**, *79*, 304–309.
- [38] M. Kuzminska, T. V. Kovalchuk, R. Backov, E. M. Gaigneaux, *J. Catal.* **2014**, *320*, 1–8.
- [39] H. M. Altass, A. E. R. S. Khder, *J. Mol. Catal. A* **2016**, *411*, 138–145.
- [40] J. Liu, Q. H. Yang, L. Zhang, H. Q. Yang, J. S. Gao, C. Li, *Chem. Mater.* **2008**, *20*, 4268–4275.
- [41] J. W. Tang, X. F. Zhou, D. Y. Zhao, G. Q. Lu, J. Zou, C. Z. Yu, *J. Am. Chem. Soc.* **2007**, *129*, 9044–9048.
- [42] Y.-B. Huang, Y. Fu, *Green Chem.* **2013**, *15*, 1095–1111.
- [43] Y. N. Sun, J. L. Hu, S. An, Q. Q. Zhang, Y. H. Guo, D. Y. Song, Q. K. Shang, *Fuel* **2017**, *207*, 136–145.
- [44] H.-J. Kim, Y.-G. Shul, H. Han, *Appl. Catal. A: Gen.* **2006**, *299*, 46–51.
- [45] J. Liu, H. Q. Yang, F. Kleitz, Z. G. Chen, T. Y. Yang, E. Strounina, G. Q. Lu, S. Z. Qiao, *Adv. Funct. Mater.* **2012**, *22*, 591–599.
- [46] Q. H. Yang, M. P. Kapoor, S. Inagaki, *J. Am. Chem. Soc.* **2002**, *124*, 9694–9695.
- [47] C. Y. Shi, Y. L. Zhao, J. Y. Xin, J. Q. Wang, X. M. Lu, X. P. Zhang, S. J. Zhang, *Chem. Commun.* **2012**, *48*, 4103–4105.
- [48] X. H. Qi, M. Watanabe, T. M. Aida, R. L. Smith Jr., *Green Chem.* **2009**, *11*, 1327–1331.
- [49] X. H. Qi, M. Watanabe, T. M. Aida, R. L. Smith Jr., *Green Chem.* **2008**, *10*, 799–805.
- [50] H. Hafizi, A. N. Chermahini, M. Saraji, G. Mohammadnezhad, *Chem. Eng. J.* **2016**, *294*, 380–388.
- [51] J. H. Dai, L. F. Zhu, D. Y. Tang, X. Fu, J. Q. Tang, X. W. Guo, C. W. Hu, *Green Chem.* **2017**, *19*, 1932–1939.
- [52] A. J. Crisci, M. H. Tucker, M.-Y. Lee, S. G. Jang, J. A. Dumesic, S. L. Scott, *ACS Catal.* **2011**, *1*, 719–728.
- [53] Y. W. Dou, S. Zhou, C. Oldani, W. H. Fang, Q. Cao, *Fuel*, **2018**, *214*, 45–54.
- [54] N. S. Shamsul, S. K. Kamarudin, N. A. Rahman, *Bioresour. Technol.* **2018**, *247*, 821–828.